Accepted Manuscript

Check for updates

Volume 54
Number 1
4 January 2018
Pages 1-112

ChemComm

Chemical Communications

rsc.li/chemcomm

ISSN 1359-7345

ROYAL SOCIETY OF CHEMISTRY

COMMUNICATION
S. J. Connon, M. O. Senge et al
Conformational control of nonplanar free base porphyrins:
towards bifunctional catalysts of tunable basicity

ROYAL SOCIETY OF CHEMISTRY

rsc.li/chemcomm

Crystallographic datasets are available from the CCDC deposition numbers 2332849, 2357823-2357832 and other analytical data can be retrieved via DOI: 10.1039/10.5061/dryad.sxksn03bf

ChemComm Accepted Manuscript

COMMUNICATION

Tetraphenylpentalenide organolanthanide complexes

Nicholas J. Katzer,[a,b,‡] Mandeep Kaur,[c,‡] Asmita Sen,[d‡] Rupal Nimaiyar,[a] Jochen Autschbach,[d*] Polly L. Arnold,[a,b*] and Ulrich Hintermair[c*]

The D_{2h} symmetrical 1,3,4,6-tetraphenylpentalenide is an excellent ligand for the stabilisation of strongly coloured bis(pentalenide) sandwich Ln^{III} complexes. These easily accessible compounds complement previously reported lanthanide sandwich organometallics and provide new opportunities to understand the roles of the f-orbitals in electronic structures.

Organometallic complexes have made major contributions to the understanding of electronic structure and bonding across the periodic table. Sandwich molecules such as ferrocene and bis(benzene) chromium have led the way and allowed for interesting applications in organic spintronics and single molecule memory storage.[1] F-block compounds in particular can display fascinating electronic properties at the quantum level including magnetism, Kondo behaviour, and superconductivity.[2-6] Fundamental studies on f-block complexes with unusual electronic structures can help explain these phenomena, potentially providing transformative breakthroughs for quantum computing and future technologies at the nano-scale.[7-12]

Surprisingly, the range of organometallic ligands with the capacity to form bonding interactions with orbitals of many different symmetries is still small and limited mostly to monocyclic aromatic hydrocarbons such as 6π cyclopentadienide ($C_5H_5^-$, **Cp**$^-$)[13] and 10π cyclooctatetraenide ($C_8H_8^{2-}$, **COT**$^{2-}$)[14] derivatives.[15] The use of bicyclic 10π pentalenide ($C_8H_6^{2-}$, **Pn**$^{2-}$; Figure 1) in f-block organometallic chemistry has grown in popularity due to its D_{2h} symmetry allowing for favorable bonding interactions involving δ-symmetry orbitals and the metal's d_{z2} which are not available in the **COT** analogues due to their D_{8h} symmetry.[16] Besides the parent **Pn**$^{2-}$ synthesised by *in-situ* deprotonation of unstable dihydropentalene,[17] 1,4-disilylated derivatives (**Pn†**)$^{2-}$ with increased stability and solubility have been reported.[18] A hexamethylated pentalenide (**Pn***)$^{2-}$ can also be accessed by a multi-step organic synthesis,[19] and more recently 1,3,4,6-tetraphenyl pentalenide (**Ph₄Pn**$^{2-}$) has been reported to be accessible through the ring-closing condensation of **Cp**'s with enones.[20, 21]
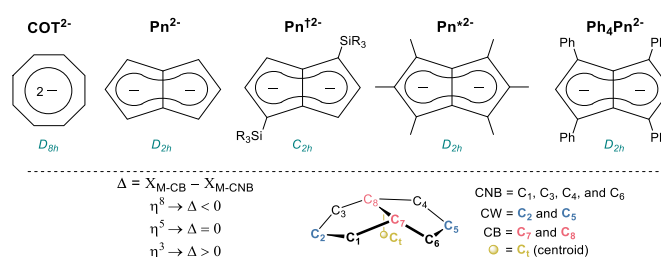

Figure 1: *Dianionic 10π ligands for organometallic complexes (upper) and positional numbering and hapticity definition of pentalenides (lower).*

Bis(η^8-pentalenide) sandwich compounds $[M(\eta^8-C_8H_n(R)_{6-n})_2]$ have been reported for Ti, Zr, Hf, Ce, Th, and U.[18] These formal 20 electron complexes typically feature a staggered conformation with some degree of folding of the pentalenide around its bridgehead carbons (CB, C_7-C_8; Figure 1).[22] We were particularly interested in the f-block chemistry of these sandwich structures such as $K[Ce^{III}(\eta^8-$**Pn***$)]_2,$[23] and M^{IV} (M = Ce, U, Th) containing $[M(\eta^8-$ **Pn†**$)]_2$ (Figure 2).[24-26] This is because the ground state electronic structure of cerocene, and also the actinocenes, has been the subject of much debate and interest.[27] In particular, comparison of the planar D_{8h} symmetrical **COT**$^{2-}$ with the folded D_{2h} symmetrical **Pn**$^{2-}$ in the stabilisation of actinide cations should offer further insight into the covalency in f-block bonding.[28-30] The ground state electronic structure of $[Ce(\textbf{COT})_2]$ is probably best viewed as a mixture of ~80 % Ce^{III} with an isolated $4f^1$ cation coupled to an unpaired electron in the ring's π orbitals, and ~20% of a state containing the Ce^{IV} ion sandwiched by two aromatic 10π dianions with significant Ce 4f–ring covalency.[31-33]

Pentalenides have also been shown to be excellent supporting ligands for pianostool f-block complexes with interesting electronic and reactivity properties. For example, $[(\eta^8-$**Pn†**$)Dy^{III}(\eta^5-$**Cp***$)]$ behaves as a single molecule magnet with an energy barrier of 245 cm^{-1}.[34] In related U^{III} complexes the fold of the **Pn**$^{2-}$ ligand was noted as important for subsequent reactivity such as dinitrogen reduction to form $(N_2)[U(\eta^5-$**Cp***$)(\eta^8-$**Pn†**$)]_2.$[35, 36]

Here we explore the organometallic lanthanide chemistry of 1,3,4,6-tetraphenylpentalenide **Ph₄Pn**$^{2-}$ with a range of 4f cations and study the metal-ligand bonding both experimentally and computationally.

a. Department of Chemistry, University of California, Berkeley, CA, 94720, USA

b. Chemical Sciences Division, Lawrence Berkeley National Laboratory, Berkeley, CA 94720, USA.

c. Department of Chemistry, University of Bath, BA2 7AY, United Kingdom.

d. Department of Chemistry, University at Buffalo, State University of New York, Buffalo, New York 14260, USA.
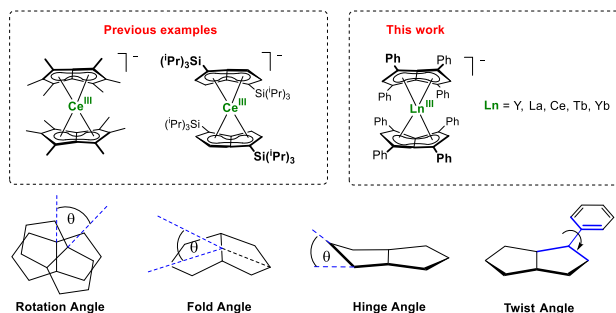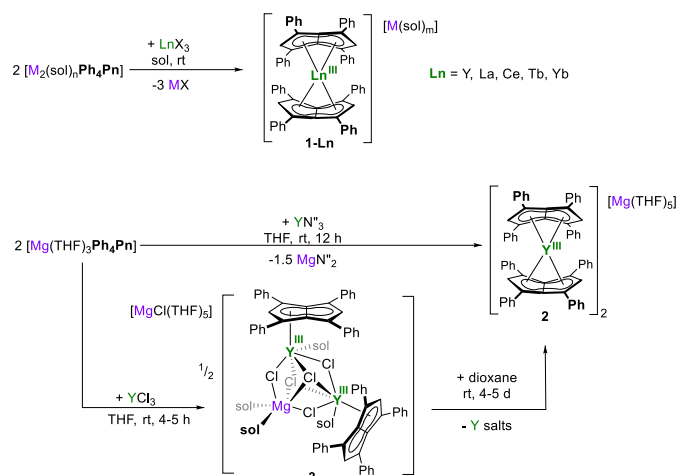
‡ Equal contributions.

ChemComm Accepted Manuscript

Figure 2: *F-block bis(pentalenide) sandwich complexes (upper) and geometric definitions of relevant structural parameters (lower).*

Scheme 1: *Synthesis of [M(sol)$_m$][Ln^{III}(Ph$_4$Pn)$_2$]$_2$ (**1-Ln**) for Ln = Y, La, Ce, Tb, Yb from group 1 pentalenide salts (for Ln=Y, M=Li, n=4, X=Cl, sol=THF, M(sol)m = Li(DME)$_3$; for Ln=Ce, M=K, n=2, X=Br, sol=DME, M(sol)m = K(DME)$_4$; for Ln=Yb, M=Na, n=6, X=Cl, sol=THF, M(sol)m = Na(THF)$_5$), synthesis of the Mg analogue of **1-Y**, [Mg(THF)$_5$][Y^{III}(Ph$_4$Pn)$_2$]$_2$ (**2**) from a magnesium pentalenide, and a half-sandwich cluster [MgCl(THF)$_5$][(Y^{III}Ph$_4$Pn)$_2$(μ-Cl)$_5$Mg(THF)$_4$] (**3**).*

Salt metathesis reactions between dilithium, disodium, or dipotassium salts of **Ph$_4$Pn^{2-}** reacted cleanly with half an equivalent of anhydrous lanthanide(III) halides in THF or DME to afford the pentalenide Ln sandwich 'ate' complexes [M(sol)$_m$][Ln^{III}(**Ph$_4$Pn**)$_2$]$_2$ (**1-Ln**) for Ln = Y (orange), La (bright orange), Ce (rust-orange), Tb (bright red), Yb (red-orange) (Scheme 1). These are a good representation of the size and Lewis acidity range for the rare earths, with r$_{covalent}$(6-coordinate Ln^{III}) = 0.900 Å (Y), 1.032 Å (La), 1.01 Å (Ce), 0.923 Å (Tb), 0.868 (Yb).[37] The reactions proceed most cleanly for the largest Ln, with isolated yields of 76 % for **1-La**, 87 % for **1-Ce**, and 77 % for **1-Tb**, but only a few single crystals could be isolated from the reaction that afforded **1-Yb**. ^{1}H NMR spectroscopic analysis of the crude product solution of the latter suggested the formation of a mixture of products, so further efforts to isolate pure material were not pursued. We have also crystallographically characterized the new DME adducts of Li$_2$[**Ph$_4$Pn**], K$_2$[**Ph$_4$Pn**], and **1-Ln** (see ESI).

Magnesium pentalenides may also be used to make rare earth pentalenide sandwich complexes.[38] A metathesis reaction between Mg[**Ph$_4$Pn**] and Y(N'')$_3$ (N'' = bis{trimethylsilyl}amide, Scheme 1) gave the magnesium congener of **1-Y**, orange [Mg(THF)$_5$][Y^{III}(**Ph$_4$Pn**)$_2$]$_2$ (**2**) in 40 % isolated yield plus Mg(N'')$_2$ as a by-product. An orange slurry of equimolar YCl$_3$ and Mg[**Ph$_4$Pn**] in THF at room temperature immediately turns red, and work-up after four hours yields the

trimetallic [Mg^{II}(Y^{III})$_2$] halide bridged complex [MgCl(THF)$_5$][(Y^{III}**Ph$_4$Pn**)$_2$(μ-Cl)$_5$Mg(THF)$_4$] (**3**, Scheme 1). The same reaction with group 1 pentalenide salts gave similar results (Figure S1), suggesting the formation of halide-bridged mono-pentalenide clusters to be characteristic of the harder Y^{III} cation.[39] Attempts to break up the halide bridges to access monomeric pianostool Y^{III} complexes by addition of AgPF$_6$, B(C$_6$F$_5$)$_3$, or AlCl$_3$ led to decomposition into unidentifiable mixtures, but **3** could be converted to the bis(pentalenide) sandwich [Mg(THF)$_5$][Y^{III}(**Ph$_4$Pn**)$_2$]$_2$ (**2**) similar to **1-Y** by addition of dioxane, as confirmed by NMR and XRD (Figure S2). All these reactions support the expectation that the bis-η^8 sandwich complexes are the thermodynamically favored products for the rare earth cations.

The ^{1}H NMR spectra of the diamagnetic **1-Ln** and **2** show diagnostic resonances for the pentalenide wingtip protons H$_w$ which are sensitive reporters for the degree of shielding of the 10π system (Figure 1).[40] Spectra of **1-La** in THF show a single resonance for the two equivalent H$_w$ at 6.39 ppm and a corresponding C$_w$ resonance at 122.5 ppm. Comparatively, the NMR spectrum of **2** in THF contained a single ^{1}H resonance for H$_w$ at 7.20 ppm and a ^{13}C resonance for C$_w$ at 124.1 ppm. The latter is 8.6 ppm higher frequency than in Mg[**Ph$_4$Pn**] which exists as a solvent-separated ion pair in an ethereal solution.[38] The NMR spectra of the cluster complex **3** also show a D$_{2h}$ symmetrical pentalenide with one sharp set of equivalent H$_w$ at temperatures down to −60 °C in THF (Figure S7) while DOSY analysis suggests the cluster anion of **3** remains intact in solution (D = 6.325 · 10^{-10} m^2/s corresponding to 1462 g/mol compared to MW = 1484 g/mol; Figure S3). These observations support the presence of strong Mg-Cl-Y interactions in the trinuclear cluster with rapid ring slippage of the η^5 pentalenide on Y^{III}.[41]

The D$_{2h}$ symmetry of 1,3,4,6-**Ph$_4$Pn^{2-}** greatly facilitates structural analysis of the new sandwich complexes in solution and in the solid state, as it eliminates the formation of *meso*, *rac*, and twist isomers seen with the C$_{2h}$ symmetrical 1,4-bis(silyl)-substituted (**Pn†**)$^{2-}$ (Figure 1).[18] **1-Ln** crystallize as either solvent-separated ion pairs (SSIP) or contact ion pairs (CIP) depending on the solvent and countercation. In each case, the Ln^{III} ion sits on a crystallographic C$_2$ axis positioned centrally between two parallel (C$_t$-Ln-C$_{t'}$ angles close to 180°) but staggered **Ph$_4$Pn^{2-}** ligands which are rotated by 38-76° against each other with noticeable inward folding by ~24° to form a hydrocarbon capsule around the metal.[24] Each C$_5$ ring of the pentalenide remains planar with no noticeable wingtip hinging, and phenyl twist angles are in the typical range of 19-49° previously observed for other s- and d-block complexes of **Ph$_4$Pn^{2-}**.[20, 38, 41] Ring slippage values of Δ = -0.3 indicate bis-η^8 coordination for all metals and M-C$_t$ distances are similar once normalized for the metal radius, except for **1-Yb** where the M-C$_t$ of 2.280 Å is anomalously long, and **2** where the M-C$_t$ of 2.048 Å is anomalously short. Both of these also have larger pentalenide rotation angles of 76.2 and 71.9° respectively, compared to an average of 38.6° for the others. **1-Ce(DME)** is shown in Figure 3 (left) as an example.

The solid-state structure of complex **3** (Figure 3, right) can be considered to comprise two [Y^{III}(**Ph$_4$Pn**)Cl$_2$]$^-$ anions linked by a [MgCl]$^+$ cation through bridging halides, with THF molecules saturating the coordination spheres of Mg^{II} and Y^{III}. In contrast to **1** and **2**, in **3** the **Ph$_4$Pn^{2-}** ligands bind to each Y^{III} in nearly perfect η^5 coordination (Δ = -0.006). The 2.319 Å Y-C$_t$ distance in **3** is significantly longer than that in **2** (2.048 Å) consistent with lower hapticity and thus weaker binding.
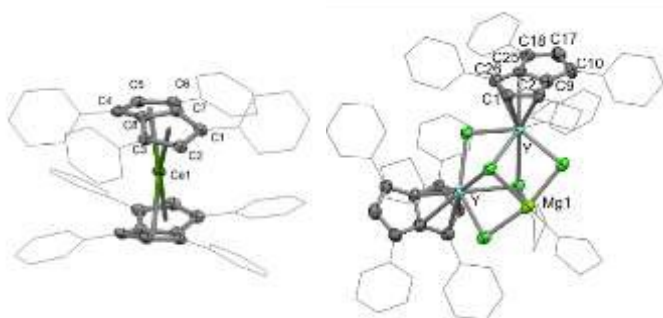
*Figure 3: Molecular structures of (left) the anion of **1-Ce**(DME) and (right) the anionic MgY2 pentalenide cluster of **3**. Selected ellipsoids drawn at 50 % probability; H atoms, counter cations and lattice solvent omitted for clarity.*

Starting from the crystal structure data, molecular geometries were optimised computationally for [Ln^{III}(η^8-**Ph$_4$Pn**)$_2$]$^-$ with Ln = La, Ce, and Tb in their respective electronic ground states with S = 0, ½, 3 using the PBE0 functional (see ESI for details).[42-44] All structures were confirmed as minima via harmonic vibrational frequency calculations, and all Ln-C distances agreed very well with those found experimentally (Figures S22-S24, S29 and Tables S1-S3 & S9-S11). Superimposing the optimized geometries on the crystal structures showed the latter to be representative of what would be found in solution (as obtained from the calculations; see Figure S25 and Table S4).

The chemical bonding and metal electronic configurations were analysed by Natural Localized Molecular Orbitals (NLMOs) and Natural Population Analysis (NPA). Each ligand has a 10-electron 5-orbital π system in the bicyclic core represented by ligand-centred NLMOs that are strongly delocalized over the pentalenide (as is typical for delocalized π-donor ligands)[40] and clearly donating electron density to the metal. For example, the ten (both ligands) relevant **1-La** NLMOs each contain 3 - 5% La character, which sums to about 0.24/0.57 electrons being donated to 4f/5d and the remainder into more diffuse shells (Table S5). At La, these NLMOs are mainly of 5d character (>50%) with secondary 4f admixtures (Figure S26). The La charge as determined by NPA is +1.85, smaller than the formal +3 charge, as expected because of ligand to metal electron donation. Optimised molecular structural data in comparison with experimental parameters are provided in Tables S1-S3, along with Ln-C Wiberg bond orders (WBOs). As suggested recently,[45] higher WBOs correlate with shorter Ln-C distances. Notably, the bridgehead carbons generate the largest WBOs within the ligand, correlating with the shortest distances to the metal. Similar bonding patterns were found in **1-Ce** and **1-Tb** (Table S5, Figures S23-S28) but we note that there is almost no donation into 4f for the Tb system, with the occupancy determined as 4f$^{0.24}$, 4f$^{1.22}$, and 4f$^{8.04}$ for La, Ce, and Tb congeners respectively. The calculations also reveal π-delocalization between the pentalenide core and the phenyl substituents as found earlier for the THF-solvated Li salts,[40] resulting in reduced ligand-to-metal donation compared to the parent **Pn^{2-}** (Table S6). The overall −1 charge of each complex is balanced by the donation between ligands and the metal, with the eight phenyl groups in each complex collectively holding a charge of about -0.5 (Table S7). We also performed comparative calculations for the analogous [Ln^{III}(η^8-**COT**)$_2$]$^-$ complexes (Table S8) which show overall the order of ligand-to-metal donation increases from **Ph$_4$Pn^{2-}** through **COT^{2-}** to **Pn^{2-}**, with most of the differences impacting the donation into 5d and more diffuse shells. The extent of donation into 4f is similar for the three types of ligands.

The experimental UV-vis-NIR spectra of **1-La**, **1-Ce** and **1-Tb** in DME are dominated by an intense absorption around 380 nm with extinction coefficients of >30,000 M^{-1}cm^{-1} (Figures 4 and S10), whereas for the Y^{III} complexes **2** and **3** in THF these transitions are slightly less intense and blue-shifted by around 30 nm (Figures S30, S32, S35). The spectra of **1-La** and **1-Ce** further feature minor lower-energy transitions around 550 and 750 nm.
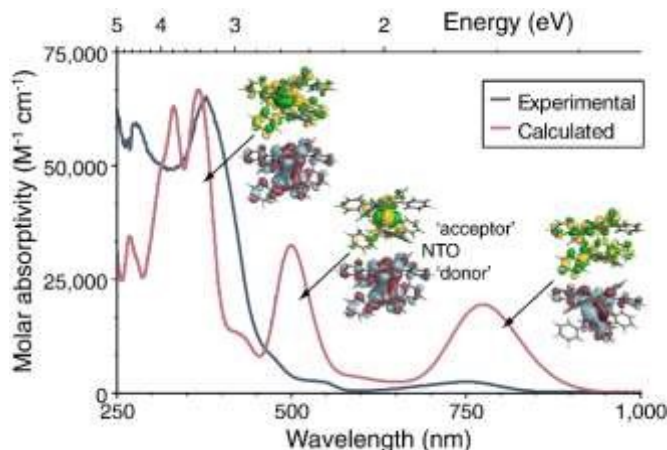

*Figure 4: UV-vis-NIR spectrum of **1-La** in DME at room temperature (dark blue). TD-DFT calculated spectrum (red). Insets: representative NTOs (isosurfaces) for the most intense transitions.*

Time-dependent DFT calculations of the electronic excitation spectra of **1-Ln** reproduced the observed spectral patterns in gas phase calculations as well as with the use of a solvent model, although at the chosen level of broadening the computed bands are more intense in the low-energy regions than the experimental spectra. The natural transition orbital (NTO) analysis of **1-La** (Figure 4 and S31) shows low-energy bands around 1.6 eV / 780 nm and 2.5 eV / 500 nm. The calculated spectrum also features comparatively intense bands at energies of 3.1 eV and higher / 400 nm and below. According to the NTO analysis, an intense transition calculated around 375 nm has mixed intra-ligand, MLCT, and metal 5d to 6p character, the latter being possible because of the donation into 5d in the ground state. The most intense transition in the 500 nm peak has mixed LMCT and 5d-5d, with the acceptor NTO of the dominant contribution to the transition having approximate δ symmetry about the C$_t$-Ln-C$_{t'}$ axis. The donor ('hole') NTO in both cases corresponds closely to the HOMO-1. The transition at lowest energy is assigned as HOMO to ligand π* with weak metal contributions in the acceptor NTO (Figures 4 and S29-S31). The peak assignment is qualitatively similar for the corresponding absorptions of **1-Ce** (Figures S32-S34) and **1-Tb** (Figures S35-S36). In contrast to the analogous **COT^{2-}** complexes, participation of the phenyl substituents is clearly noticeable in the NTOs. Furthermore, the pentalenides induce mixing of rotational symmetries of σ, π, δ, and φ where the metal and ligand fragment orbitals are similar in energy (Figures 4 and S37-S39).

In conclusion, the **Ph$_4$Pn^{2-}** ligand is highly suited for stabilising f-block organometallics giving access to both half-sandwich as well as sandwich complexes of the rare earths. Its ease of synthesis, high symmetry and ready crystallisation facilitate NMR and XRD analysis and promises access to the first homologous series of f-block pentalenide sandwich complexes to investigate fundamental aspects of electronic structure and bonding. In comparison to unsubstituted **Pn^{2-}** and **COT^{2-}** we find **Ph$_4$Pn^{2-}** to be a better acceptor, i.e. the order of ligand-to-metal electron donation (primarily into 5d orbitals) is

Pn>**COT**>**Ph₄Pn**. This will prove useful for the stabilisation of electron-rich f-block organometallics where the comparatively low symmetry offers positive overlap of ligand frontier orbitals with the metal ion's d_{z2} orbital which is not possible in the **COT²⁻** complexes.

Data availability

Electronic Supplementary Information (ESI) includes additional experimental, computational, and crystallographic details. Crystallographic datasets are available from the CCDC deposition numbers 2332849, 2357823-2357832, and other analytical data can be retrieved via DOI: 10.1039/10.5061/dryad.sxksn03bf.

Author Contributions

NJK, MK: experimental work, data analysis, visualization, draft writing and editing. RN: investigation, analysis. AS, JA: design, interpretation, and analysis of the computational studies. UH, PLA, JA: funding acquisition, project conceptualization, supervision, data analysis, visualization, manuscript writing, reviewing, and editing.

Acknowledgments

Conflicts of interest

There are no conflicts of interest to declare.

References

1. H. Werner, *Angew. Chem. Int. Ed.*, 2012, **51**, 6052.
2. S. Bart and E. Schelter, *Organometallics*, 2017, **36**, 4507.
3. L. Ungur and L. Chibotaru, *Inorg. Chem.*, 2016, **55**, 10043.
4. C. Gould, K. McClain, J. Yu, T. Groshens, et al., *J. Am. Chem. Soc.*, 2019, **141**, 12967.
5. N. Mahieu, J. Piątkowski, T. Simler and G. Nocton, *Chem. Sci.*, 2023, **14**, 443.
6. E. Castellanos and S. Demir, *Inorg. Chem.*, 2023, **62**, 2095.
7. L. Münzfeld, M. Dahlen, A. Hauser, N. Mahieu, et al., *Angew. Chem. Int. Ed.*, 2023, **62**, e202218107.
8. P. Arnold, S. Mansell, L. Maron and D. McKay, *Nature Chem.*, 2012, **4**, 668.
9. W. Huang, F. Dulong, T. Wu, S. I. Khan, et al., *Nature Commun.*, 2013, **4**, 1448.
10. S. Minasian, J. Keith, E. Batista, K. Boland, et al., *Chem. Sci.*, 2014, **5**, 351.
11. D. Smiles, E. Batista, C. Booth, D. Clark, et al., *Chem. Sci.*, 2020, **11**, 2796.
12. C. Gould, J. Marbey, V. Vieru, D. Marchiori, et al., *Nature Chem.*, 2021, **13**, 1001.
13. P. Jutzi and N. Burford, *Chem. Rev.*, 1999, **99**, 969.
14. F. Sroor, *J. Organomet. Chem.*, 2021, **948**, 121878.
15. P. Arnold, C. Halliday, L. Puig-Urrea and G. Nichol, *Inorg. Chem.*, 2021, **60**, 4162.
16. R. King, *Appl. Organomet. Chem.*, 2003, **17**, 393.
17. T. Katz and N. Acton, *J. Am. Chem. Soc.*, 1972, **94**, 3281.
18. F. Cloke, J. Green, A. Kilpatrick and D. O'Hare, *Coord. Chem. Rev.*, 2017, **344**, 238.
19. A. Ashley, A. Cowley and D. O'Hare, *Chem. Commun.*, 2007, 1512.
20. S. Boyt, N. Jenek, H. Sanderson, G. Kociok-Köhn, et al., *Organometallics*, 2022, **41**, 211.
21. N. Jenek, M. Balschun, S. Boyt and U. Hintermair, *J. Org. Chem.*, 2022, **87**, 13790.
22. K. Costuas and J.-Y. Saillard, *Chem. Commun.*, 1998, 2047.
23. A. Ashley, G. Balazs, A. Cowley, J. Green, et al., *Chem. Commun.*, 2007, 1515.
24. G. Balazs, F. Cloke, J. Green, R. Harker, et al., *Organometallics*, 2007, **26**, 3111.
25. O. T. Summerscales and F. G. N. Cloke, *Coord. Chem. Rev.*, 2006, **250**, 1122.
26. F. Cloke and P. Hitchcock, *J. Am. Chem. Soc.*, 1997, **119**, 7899.
27. O. Walter, in *Comprehensive Organometallic Chemistry IV*, eds. G. Parkin, K. Meyer and D. O'Hare, Elsevier, Oxford, 2022, pp. 582.
28. M. Neidig, D. Clark and R. Martin, *A Tribute to Edward I. Solomon on his 65th Birthday: Part 2*, 2013, **257**, 394.
29. A. Kerridge, *Chem. Commun.*, 2017, **53**, 6685.
30. S. Cooper and N. Kaltsoyannis, *Dalton Trans.*, 2021, **50**, 1478.
31. D.-C. Sergentu, C. Booth and J. Autschbach, *Chem. Eur. J.*, 2021, **27**, 7239.
32. O. Mooßen and M. Dolg, *Chem. Phys. Lett.*, 2014, **594**, 47.
33. G. Ganguly, D.-C. Sergentu and J. Autschbach, *Chem. Eur. J.*, 2020, **26**, 1776.
34. A. Kilpatrick, F.-S. Guo, B. Day, A. Mansikkamäki, et al., *Chem. Commun.*, 2018, **54 51**, 7085.
35. F. Cloke and P. Hitchcock, *J. Am. Chem. Soc.*, 2002, **124**, 9352.
36. N. Tsoureas, L. Maron, A. Kilpatrick, R. Layfield, et al., *J. Am. Chem. Soc.*, 2020, **142**, 89.
37. R. Shannon, *Acta Cryst. A*, 1976, **32**, 751.
38. H. Sanderson, G. Kociok-Köhn and U. Hintermair, *Inorg. Chem.*, 2023, **62**, 15983.
39. R. Cooper, F. Chadwick, A. Ashley and D. O'Hare, *Organometallics*, 2013, **32**, 2228.
40. N. Jenek, A. Helbig, S. Boyt, S. Reeksting, et al., *ChemRxiv*, 2023, DOI 10.26434/chemrxiv-2023-z8jdq.
41. H. Sanderson, G. Kociok-Köhn, C. McMullin and U. Hintermair, *Dalton Trans.*, 2024, **53**, 5881.
42. E. Glendening, C. Landis and F. Weinhold, *Wiley interdisciplinary reviews: computational molecular science*, 2012, **2**, 142.
43. C. Adamo and V. Barone, *Chem. Phys. Lett.*, 1998, **298**, 113.
44. E. Baerends, A. Atkins, J. Autschbach, O. Baseggio, et al., 2023.
45. E. Reinhart, C. Studvick, A. Tondreau, I. Popov, et al., *Organometallics*, 2024, **43**, 284.

ChemComm Accepted Manuscript